JCTC Journal of Chemical Theory and Computation

A Combined Charge and Energy Decomposition Scheme for Bond Analysis

Mariusz P. Mitoraj,[†,‡] Artur Michalak,[‡] and Tom Ziegler*[,†]

Department of Chemistry, University of Calgary, 2500 University Drive NW, Calgary, Alberta Canada, and Department of Theoretical Chemistry, Faculty of Chemistry, Jagiellonian University, R. Ingardena 3, 30-060 Cracow, Poland

Received November 19, 2008

Abstract: In the present study we have introduced a new scheme for chemical bond analysis by combining the Extended Transition State (ETS) method [*Theor. Chim. Acta* **1977**, *46*, 1] with the Natural Orbitals for Chemical Valence (NOCV) theory [*J. Phys. Chem. A* **2008**, *112*, 1933; *J. Mol. Model.* **2007**, *13*, 347]. The ETS-NOCV charge and energy decomposition scheme based on the Kohn−Sham approach makes it not only possible to decompose the deformation density, $\Delta\rho$, into the different components (such as σ, π, δ, etc.) of the chemical bond, but it also provides the corresponding energy contributions to the total bond energy. Thus, the ETS-NOCV scheme offers a *compact*, qualitative, and quantitative picture of the chemical bond formation within one common theoretical framework. Although, the ETS-NOCV approach contains a certain arbitrariness in the definition of the molecular subsystems that constitute the whole molecule, it can be widely used for the description of different types of chemical bonds. The applicability of the ETS-NOCV scheme is demonstrated for single (H_3X-XH_3, for X = C, Si, Ge, Sn) and multiple ($H_2X=XH_2$, $H_3CX\equiv XCH_3$, for X = C, Ge) covalent bonds between main group elements, for sextuple and quadruple bonds between metal centers (Cr_2, Mo_2, W_2, $[Cl_4CrCrCl_4]^{4-}$), and for double bonds between a metal and a main group element ($(CO)_5Cr=XH_2$, for X = C, Si, Ge, Sn). We include finally two applications involving hydrogen bonding. The first covers the adenine-thymine base pair and the second the interaction between C−H bonds and the metal center in the alkyl complex.

Introduction

Chemical bonding theory predates quantum mechanics with the work by Lewis from 1916.[1] In the Lewis picture, molecules are formed from atoms (fragments) by the grouping of electrons into lone and bonding pairs. The Lewis picture has since 1916 been consolidated and expanded upon, most often with the help of quantum mechanics. Especially useful in this regard has been the formulation of valence bond[2,3] and molecular orbital[4,5] theory.

The many useful schemes that are available for analyses of the chemical bond emphasizes different aspects of bonding. One group focuses on the charge rearrangement associated with electron pairing, as the molecule is formed from atoms (fragments). Schemes and concepts that belong to this category are Bond Order Orbitals[6,7] and the very similar Natural Bond Orbitals (NBO),[8−12] Atoms in Molecules (AIM),[13] the Electron Localization Function (ELF),[14] the Laplacian of the electron density (∇^2_ρ),[13,15] the deformation density ($\Delta\rho$),[16] population schemes,[17,18] and Charge Decomposition Analysis (CDA).[19−23]

A second group of bonding schemes puts the focus on the decomposition of the bond energy into chemically meaningful contributions. Such decomposition schemes include the Kitaura−Morokuma method,[24] the Extended Transition State (ETS) scheme,[25−27,66−69] the Block Localized Wave Function Energy Decomposition, BLW-ED, presented by Mo,[28] and the kindred Absolutely Localized Molecular Orbitals Energy Decomposition Analysis (ALMO-

* Corresponding author. E-mail: ziegler@ucalgary.ca.
[†] University of Calgary.
[‡] Jagiellonian University.

10.1021/ct800503d CCC: $40.75
Published on Web 03/02/2009

EDA) by Head-Gordon.[29] Further, the Natural Energy Decomposition Analysis (NEDA) theory by Schenter,[30] the Molecular Energy Decomposition for Atoms in Molecule by Francisco,[31] the energy decomposition schemes by Mayer,[32] Korchowiec,[33] Liu,[34] and Bagus,[35] and finally Symmetry Adapted Perturbation Theory (SAPT) scheme.[36,37]

A third useful category provides descriptors of the chemical bond in terms of bond-orders (or bond multiplicity indices). Examples are the work of Pauling,[38] Wiberg,[39] Jug,[40] Mayer,[41] and Ciosłowski,42 as well as Nalewajski, Köster, and Mrozek.[43−49]

One of several useful schemes that link the concepts of bond-order, bond-orbitals, and charge rearrangement with the deformation density is the method based on Natural Orbitals for Chemical Valence (NOCV).[50−54] In this scheme a few eigenfunctions (NOCV) of the deformation density matrix (ΔP) is used to describe bond formation of the molecules from atoms or fragments in a compact form.[50−54,56] The related eigenvalues can in addition be used as valence indices as well as a measure of the change in the density associated with bond formation. However, the NOVC scheme[50−54] does not provide information about the energetics related to the charge rearrangement.

To remedy this, we shall in the present account combine the NOCV scheme with the Extended Transition State (ETS) method.[25−27] We hope in this way to provide a compact analysis of the chemical bond in terms of orbitals (NOCVs) describing the charge rearrangement and the corresponding energy contributions from these orbitals to the chemical bond. Other schemes such as (NBO),[8−12] BLW-ED,[28] and (ALMO-EDA)[29] can be used to combine energy decomposition with charge analysis. Also, our scheme shares with other analysis methods a certain degree of arbitrariness. Thus, the bonding picture that it provides depends on the choice of fragments used to describe the formation of the combined molecule.

Nevertheless we hope in the following to illustrate that the NOCV-ETS method provides a *compact* analysis of chemical bonding. To this end we shall in the following illustrate the use of our scheme in connection with single and multiple bonds between main-group elements, between main-group elements and metals, and between two metals.

Theory

The Extended Transition State Method (ETS). Consider the formation of the molecule AB from the two fragments A^0 and B^0. Let further the heat of formation be given by $\Delta E_{int} = E_{AB} - E_A - E_B$, where E_{AB}, E_A^0, and E_B^0 are the energies of AB, A^0, and B^0, respectively. The ETS scheme[25−27] decomposes ΔE_{int} into a number of chemically meaningful components representing different steps toward the formation of AB from A^0 and B^0 as:

$$E_{AB} - E_A^0 - E_B^0 = \Delta E_{int} = \Delta E_{prep} + \Delta E_{elstat} + \Delta E_{Pauli} + \Delta E_{orb} \quad (1)$$

In the first step we distort the two fragments A^0 and B^0 from their equilibrium geometries to the structures they will have in the combined complex. The corresponding energy required for this distortion is given as ΔE_{prep} in eq 1. This term is often referred to as the distortion or preparation energy. The "distortion" might also involve the promotion of the fragments to another electronic state. We shall refer to the "distorted" fragments as A and B. The corresponding energies are E_A and E_B, respectively. Thus, $\Delta E_{prep} = E_A + E_B - E_A^0 - E_B^0$.

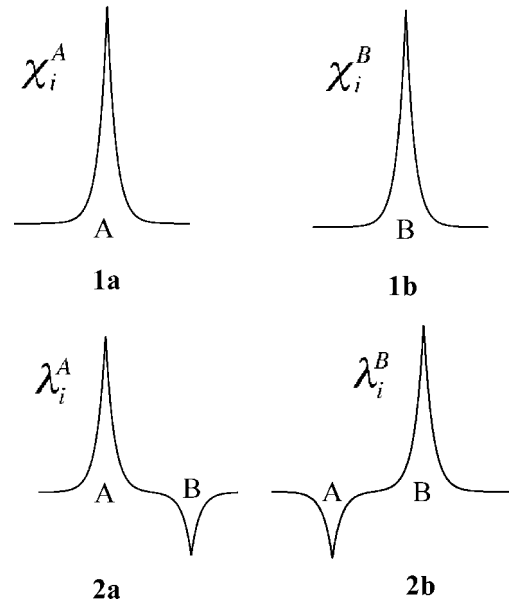

Figure 1. Schematic representation of fragment orbitals on A and B without Löwdin orthogonalization (1a, 1b) and with Löwdin orthogonalization (2a, 2b).

In the Kohn−Sham theory, A and B are represented by the Slater determinants Ψ^A and Ψ^B, respectively. Here Ψ^A is built from the occupied one-electron spin orbitals of fragment A, $\{\chi_j^A, j = 1,n_A\}$, and Ψ^B from the corresponding set on B, $\{\chi_k^B, k = 1,n_B\}$. We illustrate in Figure 1 a fragment orbital χ_j^A as **1a** and a fragment orbital χ_k^B as **1b**. Further, the occupied orbitals making up Ψ^A and Ψ^B form the set $\{\chi_i = 1,n\}$ with $n = n_A + n_B$.

In the second step we bring the distorted fragments from infinite separation to their final positions in the combined compound without changing their densities, ρ_A and ρ_B. The associated energy change $\Delta\tilde{E}^0$ due to this step is given by

$$\Delta\tilde{E}^0 = \Delta E_{elstat} + \Delta E_{XC}^0 \quad (2)$$

Here

$$\Delta E_{elstat} = \sum_{\substack{\nu\in A \\ \mu\in B}} \frac{Z_\nu Z_\mu}{R_{\nu\mu}} + \sum_{\mu\in A}\int \frac{\rho_B(r)Z_\mu}{|R_\mu - r|}dr + \sum_{\nu\in B}\int \frac{\rho_A(r)Z_\mu}{|R_\nu - r|}dr + \int\frac{\rho_A(r_1)\rho_B(r_2)}{r_{12}}dr_1dr_2 \quad (3)$$

represents the change in electrostatic interaction energy when the two distorted fragments are combined in the final molecule while the densities are kept frozen. On the other hand ΔE_{XC}^0 represents the corresponding change in the Kohn−Sham exchange correlation energy[25]

$$\Delta E^0_{XC} = \sum_{\gamma}^{\alpha\beta}\sum_{\tau}^{\alpha\beta}\{E^{\gamma,\tau}_{XC}[(\rho^{\gamma}_A + \rho^{\gamma}_B);(\rho^{\tau}_A + \rho^{\tau}_B)] - E^{\gamma,\tau}_{XC}[\rho^{\gamma}_A;\rho^{\tau}_A] - E^{\gamma,\tau}_{XC}[\rho^{\gamma}_B;\rho^{\tau}_B]\} \quad (4)$$

Here ρ^{τ}_A,ρ^{τ}_B with $\tau = \alpha,\beta$ are the spin densities of A and B, respectively. The electrostatic contribution ΔE_{elstat} enters as the second term in the expression for ΔE_{tot} of eq 1.

It is readily seen that $\tilde{E}^0 = E^0_A + E^0_B + \Delta E_{prep} + \Delta E_{elst} + \Delta E^0_{XC}$ corresponds to the energy of the simple product wave function $\Psi^A\Psi^B$. However, $\Psi^A\Psi^B$ is not antisymmetric with respect to the interchange of all electron indices. As a consequence it does not fully satisfy the Pauli exclusion principle. The product function $\Psi^A\Psi^B$ is further not normalized if the occupied orbitals on the different fragments A and B overlap.

In the third step we construct from $\Psi^A\Psi^B$ the normalized and antisymmetrized wave function

$$\Psi^0 = N\hat{A}\{\Psi^A\Psi^B\} \quad (5)$$

with the corresponding energy E^0.

The wave function Ψ^0 can[24−27] in Kohn−Sham theory be represented by a single Slater determinant as

$$\Psi^0 = |\lambda_1\lambda_2,...\lambda_i\lambda_j,...\lambda_n| \quad (6)$$

where the set $\{\lambda_i;i = 1,n\}$ is obtained from $\{\chi_i;i = 1,n\}$ by a Löwdin orthogonalization[55] and given by

$$\lambda_i = \sum_j S^{-1/2}_{ij}x_j \quad (7)$$

Here, S is the overlap matrix for the set $\{\chi_i = 1,n\}$. We illustrate in Figure 1a fragment orbital λ^A_j as **2a** and a fragment orbital λ^B_k as **2b**. Further, the density corresponding to ψ^0 can be written as:

$$\rho^0 = \sum_i^n \lambda^*_i\lambda_i = \sum_i^n\sum_j^n S_{ij}\chi_i\chi_j = \sum_i^n\sum_j^n \Delta P^{Pauli\,i}_{ij}\chi_i\chi_j + \rho^A + \rho^B \quad (8)$$

Here ΔP^{Pauli} is the (deformation) density matrix in the basis $\{\chi_i = 1,n\}$ representing the Pauli deformation density $\Delta\rho^{Pauli} = \rho^0 - \rho^A - \rho^B$. It follows from eq 8 that $\Delta P^{Pauli}_{ij} = (S_{ij} - \delta_{ij})$.

It is readily shown[25] that the energy difference $\Delta\tilde{E}_{Pauli} = E^0 - \tilde{E}^0$ between ψ^0 and $\psi^A\psi^B$ can be expressed as

$$\Delta\tilde{E}_{Pauli} = E^0[\rho^0] - E^A[\rho^A] - E^B[\rho^B] = \sum_i^{occ}\sum_j^{occ}\Delta P^{Pauli}_{ij}F_{ij}[\rho^{Pauli}_T] \quad (9)$$

where $\rho^{Pauli}_T = 1/2^0_\rho + 1/2\rho_A + 1/2\rho_B$, whereas the Kohn−Sham matrix elements are given as:

$$F_{ij}[\rho] = \int x_i(1)\{-1/2\nabla^2 + V_{Ne}(1) + V_C[\rho]\}x_j(1)d\tau_1 \quad (10)$$

where $\rho = \rho_T$. In eq 10), $V_C[\rho]$ is the Coulomb potential due to ρ and $V_{XC}[\rho]$ is the corresponding exchange correlation potential, whereas $V_{Ne}(1)$ is the nuclear-electron attraction potential due to all the atoms of the combined molecule. We note that eq 10 is derived by expanding $E^0 = E[\rho^0]$ on the one hand and $\tilde{E}^0 = E[\rho^A + \rho^B]$ on the other from the density $\rho^{Pauli}_{TS} = 1/2^0_\rho + 1/2(\rho^A + \rho^B)$ at the midpoint (transition state) between ρ^0 and $\rho^A + \rho^B$.[25] It is customary[24,25] to combine $\Delta\tilde{E}_{Pauli}$ of eq 9 and Δ^0_{XC} of eq 4 into the total Pauli or "exchange repulsion" term[24] ΔE_{Pauli} as

$$\Delta E_{Pauli} = \Delta\tilde{E}_{Pauli} + \Delta E^0_{XC} \quad (11)$$

We note that ΔE_{Pauli} enters as the third contribution to ΔE_{tot} in eq 1. It follows further from the derivation so far that $E^0 - E^0_A - E^0_B = \Delta E_{prep} + \Delta E_{elstat} + \Delta E_{Pauli}$.

The total Pauli repulsion ΔE_{Pauli} of eq 11 is dominated by $\Delta\tilde{E}_{Pauli}$ of eq 9 which is positive and destabilizing. The destabilization comes from the extra nodes added to $\{\lambda_i;i = 1,n\}$, see **2a** and **2b** of Figure 1, compared to $\{\chi_i;i = 1,n\}$, see **1a** and **1b** of Figure 1, in order to make the set $\{\lambda_i;i = 1,n\}$ orthogonal and satisfy the Pauli exclusion principle through Ψ^0. Thus, the added nodes will cause the energy of ψ^0 to be higher than that of $\Psi^A\Psi^B$ due to an increase of the kinetic energy.[24,25] The term ΔE_{Pauli} is in general responsible for an increase in the kinetic energy when chemical bonds are formed.[57]

It is customary[26,27] to combine ΔE_{Pauli} and ΔE_{elstat} under the heading of steric interaction energy as $\Delta E_{steric} = \Delta E_{Pauli} + \Delta E_{elstat}$. Defined in this way, ΔE_{steric} represents the total interaction energy between the two fragments described alone by their occupied orbitals according to Ψ^0 of eq 5 without any involvement of virtuals. This definition is especially meaningful for the interaction between neutral fragments where ΔE_{steric} invariably is positive.[69,72] The definition is consistent with the picture of steric interactions as originating from the penetrations of two electronic charge clouds ρ_A and ρ_B. Such a penetration leads to an increase in kinetic energy due to ΔE_{Pauli}. However, the increase in kinetic energy is to some degree compensated for by ΔE_{elstat}. This interaction, as defined in eq 3, is normally attractive for neutral fragments,[69,72] as the density ρ_A on one fragment only partially can shield the stabilizing (attractive) interaction of the nuclei on the same fragment A with the density ρ_B on the other fragment. In qualitative theories such as the Hückel method, ΔE_{elstat} is considered to be zero and ΔE_{Pauli} represents the steric interaction. However from a quantitative point of view, such an approximation is too severe. The two terms ΔE_{elstat} and ΔE_{Pauli} give rise to two large numbers of opposite sign that increases numerically as the fragments A and B are brought closer together. On the other hand, their sum ΔE_{steric} is numerically much smaller and chemically meaningful.

For the interaction of charged fragments one might modify ΔE_{elstat} as $\Delta E_{elstat} = \Delta\tilde{E}_{elstat} + V_{AB.}$ Here V_{AB} is an effective potential describing the interaction of the net charges on the two fragments. In that case $\Delta\tilde{E}_{steric} = \Delta\tilde{E}_{elstat} + \Delta E_{Pauli}$. Futher, V_{AB} would have to be added as an extra term to the total bonding energy. Such a modification has not been implemented yet. At the moment we can only say that for the interaction of charged fragments, ΔE_{steric} as defined above contains both $\Delta\tilde{E}_{steric}$ and V_{AB}. Of the many examples given

in the following, only the one dealing with $[Cl_4CrCrCl_4]^{4-}$ involves charged fragments. We shall qualify the use of ΔE_{steric} when we discuss $[Cl_4CrCrCl_4]^{4-}$.

The last term of eq 1, ΔE_{orb}, is called the orbital interaction term. It represents the interactions between the occupied molecular orbitals on one fragment with the unoccupied molecular orbitals of the other fragment, as well as the mixing of occupied and virtual orbitals within the same fragment (intrafragment polarization). The orbital interaction term represents the energy change when going from the Ψ^0 state, characterized by the density matrix P^0 to the final wave function, Ψ, characterized by P and the density ρ. A full expression for ΔE_{orb} will be given shortly after a discussion of the deformation density $\Delta\rho = \rho - \rho^0$.

Natural Orbitals for Chemical Valence (NOCV) and the Extended Transition State Method (ETS). In the Natural Orbitals for Chemical Valence (NOCV) approach[50−54] the deformation density

$$\Delta\rho^{orb} = \rho - \rho^{o} = \sum_{\mu}^{N}\sum_{\nu}^{N}\Delta P_{\mu\nu}^{orb}\lambda_\mu\lambda_\nu \qquad (12)$$

is expressed in terms of a set of orthonormal fragment spin−orbitals $\{\lambda_i;i = 1,N\}$ with $N = n + nv$. This set is generated by a separate Löwdin orthogonalization of the n occupied fragment orbitals $\{\chi_i;i = 1,n\}$ and nv virtual fragment orbitals $\{\chi_j;j = n + 1,n + nv\}$, followed by a Schmidt orthogonalization of the virtual set on the occupied set. The set $\{\lambda_i = i = 1,n + nv\}$ includes the occupied and orthonormal fragment orbitals $\{\lambda_i;i = 1,n\}$ introduced previously as well as a an additional set of virtual fragment orbitals $\{\lambda_i;i = 1 + 1,n + nv\}$ that are orthogornal to each other and the occupied set $\{\lambda_i;i = 1,n\}$. The Schmidt (rather than Löwdin) orthogonalization of all virtual orbitals on the occupied ensures that ρ^0 is represented by a diagonal matrix within the set $\{\lambda_i;i = n + 1,n + nv\}$.

The NOCVs are now constructed by a diagonalization of the deformation density matrix $\Delta P_{\mu\nu}^{orb}$ of eq 12 expressed in the set of orthogonalized fragment spin−orbitals. Thus, the NOCVs satisfy the equation:

$$\Delta P^{orb}C_i = v_i C_i \qquad (13)$$

where C_i is a vector containing the coefficients that expands ψ_i in the basis of orthogonalized fragment orbitals λ_j as $\psi_i = \sum_j C_{ij}\lambda_j$.

The deformation density, $(\Delta\rho^{orb})$, can in the NOCV representation be expressed as a sum of pairs of complementary orbitals (ψ_{-k}, ψ_k) corresponding to eigenvalues equal in absolute value but opposite in signs:[50−54]

$$\Delta\rho^{orb}(r) = \sum_{k=1}^{N/2} v_k[-\Psi_{-k}^2(r) + \Psi_k^2(r)] = \sum_{k=1}^{N/2}\Delta\rho_k(r) \qquad (14)$$

The structure of the eigenvalues in complementary pairs is a consequence of the fact that the set λ is orthonormalized and that ΔP is traceless. The complementary pairs of NOCV define the channels for electron charge transfer between the molecular fragments.[50−54] This "pairing" property is also characteristic for Inter-Reactant-Modes (the charge-flow channels describing changes in atomic populations) defined within the Charge Sensitivity Analysis by Nalewajski et al.[96,97]

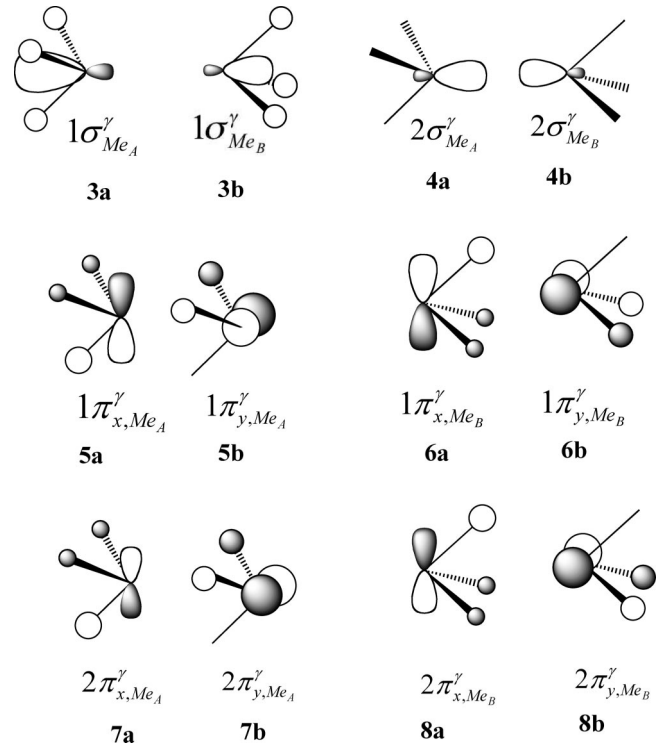

Figure 2. Schematic representation of fragment spin−orbitals in the two methyl radicals Me_A and Me_B.

We can further combine the NOCV and ETS methods in a ETS-NOCV charge and energy decomposition scheme by providing an expression for ΔE_{orb}.

The term ΔE_{orb} is given by:

$$\Delta E_{orb} = E[\rho] - E[\rho^0] \qquad (15)$$

where $E[\rho]$ is the energy of the final molecule and $E[\rho^0]$ is the energy E^0 associated with Ψ^0 of eq 6. An expansion of $E[\rho] = E[\rho^0 + \Delta\rho^{orb}]$ as well as $E[\rho^0]$ from the density $\rho^{TS} = 1/2\rho + 1/2\rho^0$ at the midpoint (transition state) between ρ and ρ^0 allows us to express ΔE_{orb} as:

$$\Delta E_{orb} = \sum_{\nu}^{N}\sum_{\mu}^{N}\Delta P_{\mu\nu}^{orb}F_{\mu\nu}^{TS} = Tr(\Delta P^{orb}F^{TS}) \qquad (16)$$

Here $\Delta P_{\mu\nu}^{orb}$of eq 16 is over orthogonalized Löwdin orbitals $\{\lambda_\mu = 1,N\}$ and $F_{\mu\nu}^{TS}$ is a matrix element similar to that of eq 10 with $\rho = \rho^{TS}$ and χ replaced by λ.

It follows from eq 13 that the NOCVs (ψ_i) are related to the set λ by a unitary transformation C. We can thus write:

$$\Delta E_{orb} = Tr(\Delta P^{orb}F^{TS}) = Tr(C^{+}\Delta P^{orb}CC^{+}F^{TS}C) = \sum_{k=1}^{N/2} v_k[-F_{-k,-k}^{TS} + F_{k,k}^{TS}] = \sum_{k=1}^{N/2}\Delta E_k^{orb} \qquad (17)$$

where C diagonalizes ΔP^{orb}. Further, $F_{-k,-k}^{TS}$ and $F_{k,k}^{TS}$ are diagonal matrix elements of the type defined in eq 10 over ψ_{-k} and ψ_k, respectively, with $\rho = \rho^{TS}$. Also eq 17 makes

Table 1. ETS-NOCV Energy Decomposition of the X−X Bond in H_3X-XH_3[a]

X	ΔE_{Pauli}	ΔE_{elstat}	ΔE_{steric}[b]	$\Delta E_{orb}{}^{\sigma}$[c]	$\Delta E_{orb}^{\pi x}$	$\Delta E_{orb}{}^{\pi y}$	$\Delta E_{orb}{}^{\pi}$[d]	ΔE_{orb}[e]	ΔE_{prep}	ΔE_{int}[f]	d(XX)[g]
C	205.9	−129.3	76.5	−173.3	−7.2	−7.2	−14.4	−187.7	17.8	−93.4	1.53
Si	97.1	−79.3	17.8	−88.3	−2.0	−2.0	−4.0	−92.3	0.6	−73.9	2.35
Ge	107.9	−88.5	19.4	−84.4	−2.0	−2.0	−4.0	−88.4	0.6	−68.4	2.43
Sn	93.7	−84.1	9.6	−66.6	−1.2	−1.2	−2.4	−69.0	0.4	−59.0	2.82

[a] kcal/mol. [b] The total steric repulsion, $\Delta E_{steric} = \Delta E_{Pauli} + \Delta E_{elstat}$. [c] The total stabilization energy from the σ-orbital interactions illustrated in Figure 4 for X = C. [d] The total stabilization energy from the π-orbital interactions illustrated in Figure 5 for X = C, $\Delta E_{orb}^{\pi} = \Delta E_{orb}^{\pi x} + \Delta E_{orb}^{\pi y}$. [e] $\Delta E_{orb} = \Delta E_{orb}^{\sigma} + \Delta E_{orb}^{\pi}$. [f] $\Delta E_{int} = \Delta E_{steric} + \Delta E_{prep} + \Delta E_{orb}$. [g] XX bond lengths in angstroms.

use of the fact that the trace of the product of two matrices is invariant to a unitary transformation of the two matrices.

The advantage of the expression for ΔE_{orb} in terms of NOCVs, eq 17, rather than orthogonalized fragment orbitals, eq 16, is that only a few complementary pairs might contribute significantly to ΔE_{orb} whereas the contributions to ΔE_{orb} in eq 16 might come from several products of orthogonalized Löwdin orbitals. We see further that for each complementary NOCV pair, representing one of the charge delocalization $\Delta\rho_k$, not only can we visualize $\Delta\rho_k$ but also provide the energy contributions ΔE_{orb}^k to the bond energy from $\Delta\rho_k$.

Computational Details

All the DFT calculations presented here were based on the Amsterdam Density Functional (ADF) program.[58−62] The Becke−Perdew exchange-correlation functional[63,64] was applied. A standard double-ζ STO basis with one set of polarization functions was adopted for the elements H, C, N, O, Si, Cl while a standard triple-ζ basis set was employed for the transition metals, Cr, Mo, W, and for the heavier main group elements, Ge, Sn. Auxiliary *s, p, d, f,* and *g* STO functions, centered on all nuclei, were used to fit the electron density and obtain accurate Coulomb potentials in each SCF cycle. Relativistic effects were included using the ZORA approximation.[65−67]

Results and Discussion

Single Bonds between the Main-Group Elements, H_3X-XH_3. Let us first analyze the formation of a single X−X bond in H_3X-XH_3, where X = C, Si, Ge, Sn. We consider X_2H_6 formed from the two radicals $H_3X^{\uparrow}$ and $^{\downarrow}XH_3$ of opposite spin.

Starting with X = C, the first step in the formation of the H_3C-CH_3 single-bond is the distortion of the two methyl radicals from their equilibrium geometry to the structure that they have in the combined molecule. The associated energy is given by ΔE_{prep} of eq 1 and amounts to a destabilization of ΔE_{prep} = 17.8 kcal/mol, Table 1. The distortion is the result of steric interactions between the two methyl fragments in H_3C-CH_3. The distortion energy is seen to be much smaller for the heavier congeners X = Si, Ge, and Sn where the distance between the two H_3X fragments in the combined X_2H_6 compound is much larger, Table 1.

The second step involves bringing the distorted fragments, $H_3C^{\uparrow}$ and $^{\downarrow}CH_3$, from infinity to their final positions in the molecule, without any change in their electronic densities. This step gives rise to the electrostatic interaction ΔE_{elstat} of eq 1. This interaction, as defined in eq 3, is normally attractive for neutral fragments, as the density on one fragment only partially can shield the stabilizing (attractive) interaction of the nuclei on the same fragment with the density on the other fragment. The reduced shielding is due to interpenetration of the two fragment densities. For C_2H_6 the contribution from ΔE_{elstat} amounts to −129.3 kcal/mol, Table 1. For the higher congeners ΔE_{elstat} becomes less stabilizing from Si to Sn as the interpenetration decreases with increasing X−X bond distance, Table 1.

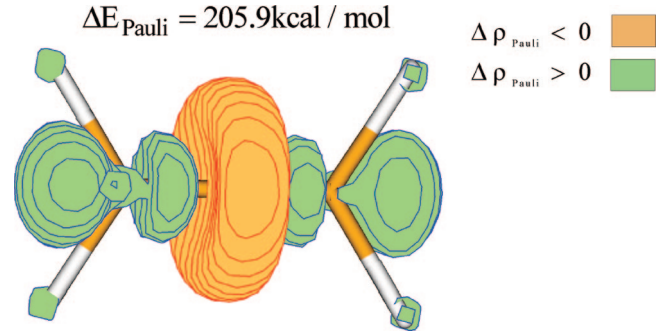

Figure 3. The contour of the Pauli deformation density $\Delta\rho^{Pauli}$ for C_2H_6. The numerically smallest contour values are ±0.01 a.u. The corresponding Pauli repulsion energy is ΔE_{Pauli} = 205.9 kcal/mol.

In the third step we construct the Kohn−Sham Slater determinant Ψ^0 of eq 6 from the orthogonalized set of occupied orbital $\{\lambda_i; i = 1,n\}$. The orbital λ_i consists of χ_i with an out-of-phase contribution from all occupied orbitals of the same spin residing on other fragments, see Figure 1. The out-of-phase contribution will make ΔE_{Pauli} of eq 11 positive. We say that occupied orbitals $\{\chi_i; i = 1,n\}$ of the same spin but on different fragments interact, destabilizing each other. Futher, ΔE_{Pauli} has contributions from both spins so that $\Delta E_{Pauli} = \Delta E_{Pauli}^{\alpha} + \Delta E_{Pauli}^{\beta}$.

In C_2H_6 the leading contribution to ΔE_{Pauli} is from the repulsive interaction between the SOMO $2\sigma_{Me_A}^{\alpha}$ (**4a** for $\gamma = \alpha$) on fragment A with a C−H bonding orbital $1\sigma_{Me_B}^{\alpha}$ (**3b** for $\gamma = \alpha$) on the other fragment as well as the SOMO $2\sigma_{Me_B}^{\beta}$ (**4b** for $\gamma = \beta$) on fragment B interacting repulsively with $1\sigma_{Me_A}^{\beta}$ (**3a** for $\gamma = \beta$) on the other fragment, see Figure 2. Another contribution is from the destabilizing interactions of the two occupied C−H bonding orbitals $1\pi_{x,Me_A}^{\gamma}$; $1\pi_{y,Me_A}^{\gamma}$ (**5a**,**b**) on one fragment with the corresponding occupied $1\pi_{x,Me_B}^{\gamma}$; $1\pi_{y,Me_B}^{\gamma}$orbitals (**6a**,**b**) on the other fragment for $\gamma = \alpha,\beta$; see Figure 2.

The changes in the electron density, $\Delta\rho^{Pauli}$, due to the Pauli interaction are presented in Figure 3. We can clearly see the outflow of the electron density from the bonding region due to the antibonding nature of the set $\{\lambda_i; i = 1,n\}$.

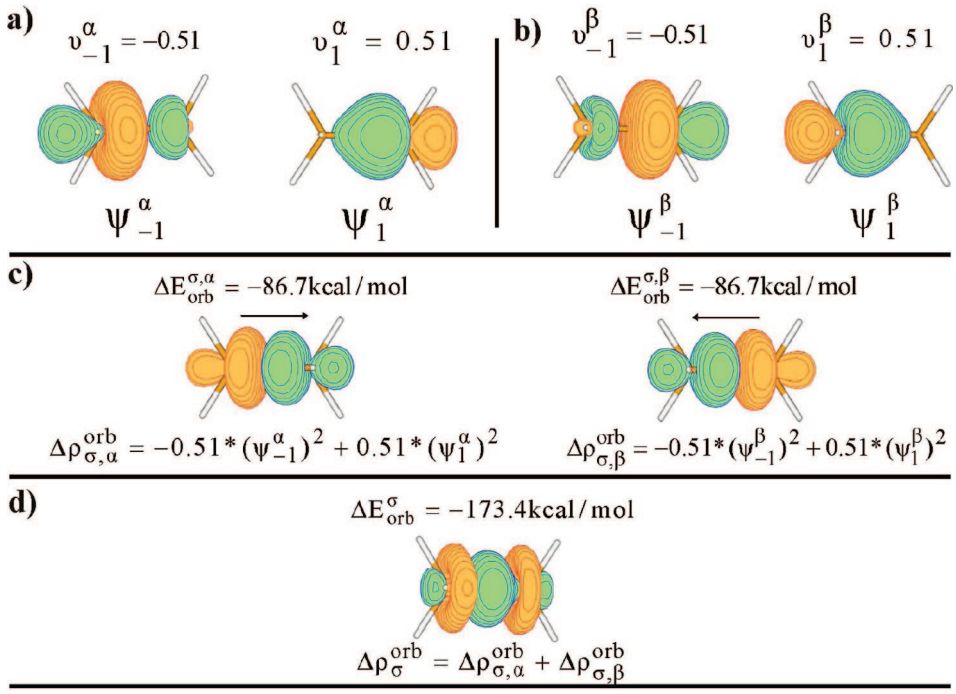

Figure 4. (a) Contours of complementary NOVCs (ψ^{α}_{-1},ψ^{α}_{+1}) representing donation from Me_A (left) to Me_B (right) and corresponding eigenvalues (υ^{α}_{-1},υ^{α}_{+1}) in C_2H_6. The numerically smallest contour values are ±0.1 a.u. (b) Contours of complementary NOVC's (ψ^{β}_{-1},ψ^{β}_{+1}) representing donation from Me_B (right) to Me_A (left) and corresponding eigenvalues (υ^{β}_{-1},υ^{β}_{+1}) in C_2H_6. The numerically smallest contour values are ±0.1 a.u. (c) Contours of sigma donation ($\Delta\rho^{orb}_{\sigma,\alpha}$) from Me_A to Me_B (left) and sigma donation ($\Delta\rho^{orb}_{\sigma,\beta}$) from Me_B to Me_A (right). The smallest contour values are ±0.0 a.u. The corresponding orbital stabilization energies are $\Delta E^{\sigma,\alpha}_{orb} = \Delta E^{\sigma,\beta}_{orb} = -86.7$ kcal/mol. (d) Total sigma donation $\Delta\rho^{orb}_{\sigma} = \Delta,\rho^{orb}_{\sigma,\alpha} + \Delta\rho^{orb}_{\sigma,\beta}$ and corresponding stabilization energies $\Delta E^{\sigma}_{orb} = \Delta E^{\sigma,\alpha}_{orb} + \Delta E^{\sigma,\beta}_{orb} = -173.4$ kcal/mol. The smallest contour values are ±0.01 a.u.

In other words, the antisymmetrization of the wave function in eq 6 reduces the electron density in the overlap region.[69] It follows from Table 1 and Figure 3 that the corresponding energy change due to the Pauli repulsion is $\Delta E_{Pauli} = 205.9$ kcal/mol. For the higher congeners, ΔE_{Pauli} becomes less repulsive from Si to Sn as the X−X bond distance increases and the overlaps between occupied orbitals on different fragments become smaller, Table 1. It follows from Table 1 that $\Delta E_{steric} = \Delta E_{Pauli} + \Delta E_{elstat}$ is destabilizing due to ΔE_{Pauli}. It is further seen that ΔE_{steric} decreases for X_2H_6 from X = C to X = Sn as the X−X bond length increases.

The final step in the $H_3C{-}CH_3$ bond formation is the inclusion of the virtual fragment orbitals on $H_3C^{\uparrow}$ and $^{\downarrow}CH_3$. The result is the density change $\Delta\rho^{orb}$ defined in eqs 12−14. Associated with $\Delta\rho^{orb}$ is the energy change ΔE_{orb} of eq 1 which is defined in eqs 15−17. The most important contributions to $\Delta\rho^{orb}$ and ΔE_{orb} are due to the in-phase interaction of the virtual orbital $2\sigma^{\beta}_{Me_A}$ (**4a** for $\gamma = \beta$) on A with the destabilized SOMO $2\sigma^{\beta}_{Me_B}$ (**4b** for $\gamma = \beta$) on fragment B, giving rise to a transfer of charge ($\Delta\rho^{orb}_{\sigma,\beta}$) from B to A as well as the interaction of the destabilized SOMO $2\sigma^{\alpha}_{Me_A}$ (**4a** for $\gamma = \alpha$) on A with the virtual orbital $2\sigma^{\alpha}_{Me_B}$ (**4b** for $\gamma = \alpha$) on B resulting in the transfer of charge from A to B ($\Delta\rho^{orb}_{\sigma,\alpha}$). The two interactions are combined responsible for the formation of the σ-bond.

The two complementary Natural Orbitals for Chemical Valence (NOCV) responsible for the σ-transfer of density from A to B are shown as ψ^{α}_{-1},ψ^{α}_{1} in Figure 4a whereas the complementary NOVC's representing the σ-transfer of density from B to A are shown as (ψ^{β}_{-1},ψ^{β}_{1}) in Figure 4b. Figure 4c holds the σ-deformation density for the A-to-B transfer given as $\Delta\rho^{orb}_{\sigma,\alpha} = -0.51(\psi^{\alpha}_{-1})^2 + 0.51(\psi^{\alpha}_{1})^2$ with the corresponding orbital stabilization energy $\Delta E^{\sigma,\alpha}_{orb} = -86.7$ kcal/mol as well as σ-deformation density for the B-to-A transfer given as $\Delta\rho^{orb}_{\sigma,\beta} = -0.51(\psi^{\beta}_{-1})^2 + 0.51(\psi^{\beta}_{1})^2$ with the corresponding orbital stabilization energy $\Delta E^{\sigma,\beta}_{orb} = -86.7$ kcal/mol. We have finally presented in Figure 4d the total σ-orbital deformation density $\Delta\rho^{orb}_{\sigma} = \Delta\rho^{orb}_{\sigma,\alpha} + \Delta\rho^{orb}_{\sigma,\beta}$ along with the total σ-orbital interaction energy $\Delta E^{\sigma}_{orb} = -173.4$ kcal/mol. The term ΔE^{σ}_{orb} clearly represents the σ-orbital interaction energy associated with the formation of the σ-bond. It follows further from Table 1 that ΔE^{σ}_{orb} decreases for X_2H_6 from X = C to X = Sn as the X−X bond length increases.

There is one more stabilizing orbital interaction, ΔE^{σ}_{orb}, that contributes to ΔE_{orb} in eq 1. It involves a transfer (polarization) from the occupied and destabilized C−H bonding orbitals $1\pi^{\gamma}_{x,Me_A}$; $1\pi^{\gamma}_{y,Me_A}$ (**5a**,**b**) and $1\pi^{\gamma}_{x,Me_B}$; $1\pi^{\gamma}_{y,Me_B}$ (**6a**,**b**) to the virtual C−H antibonding orbitals $2\pi^{\gamma}_{x,Me_A}$; $2\pi^{\gamma}_{y,Me_A}$ (**7a**,**b**) and $2\pi^{\gamma}_{x,Me_B}$; $2\pi^{\gamma}_{y,Me_B}$ (**8a**,**b**), where λ can be either α or β, see Figutre 2. Although these fragment orbitals involve C−H σ (**5**,**6**) and C−H σ^* (**7**,**8**) components, they are in accord with common practice given the designation π to emphasize the transformation properties of the contributing p-orbital combinations on the carbons. The term ΔE^{π}_{orb} does not represent the formation of a π-bond but rather a relief of repulsive Pauli interaction between occupied C−H bonding fragment orbitals on opposite fragments by donating

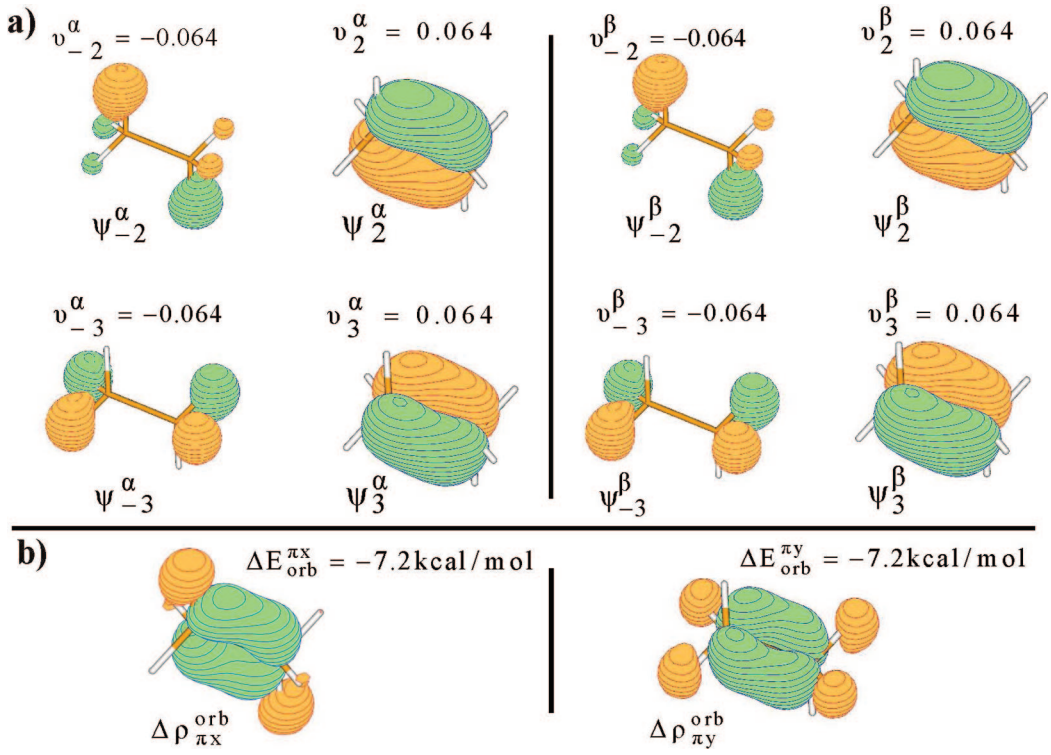

Figure 5. (a) Contours of the π-type NOCVs in C_2H_6. The numerically smallest contour values are ± 0.1 a.u. (b) The π-deformation density contributions, $\Delta\rho^{orb}_{\pi x}$, $\Delta\rho^{orb}_{\pi y}$, and corresponding energies $\Delta E^{\pi x}_{orb}$, $\Delta E^{\pi y}_{orb}$. The numerically smallest contour values are ± 0.005 a.u.

Table 2. ETS-NOCV Energy Decomposition of the Double X=X Bond in the C_2H_4 and Ge_2H_4 Systems[a]

X	ΔE_{steric}[b]	ΔE^{σ}_{orb}	ΔE^{π}_{orb}[a]	ΔE^{π}_{orb}[b]	ΔE_{orb}[c]	ΔE_{prep}[d]	ΔE_{int}[e]	d(XX)[f]
C	107.9	−220.6	−67.8	−5.7	−294.1	6.5	−179.7	1.33
Ge-planar	27.1	−76.3	−22.0	−3.0	−101.3	51.2	−23.0	2.27
Ge-bent	22.0	−75.2	−37.0	−2.6	−114.8	51.9	−40.9	2.37

[a] kcal/mol. [b] The total steric repulsion, $\Delta E_{steric} = \Delta E_{Pauli} + \Delta E_{elstat}$. [c] $\Delta E_{orb} = \Delta E^{\sigma}_{orb} + \Delta E^{\pi 1}_{orb} + \Delta E^{\pi 2}_{orb}$. [d] The distortion (or preparation) term includes the difference in energy between the singlet ground state and the triplet excited state of GeH_2 fragments. [e] $\Delta E_{int} = \Delta E_{steric} + \Delta E_{prep} + \Delta E_{orb}$. [f] XX bond lengths in angstroms.

density from these orbitals (**5**,**6**) to the virtual (**7**,**8**) pair. In this process we are trading C−H bonding and C−C antibonding interactions with C−H antibonding and C−C bonding interactions.

We give in Figure 5a the complementary pairs of NOCVs $(\psi^{\gamma}_{-2},\psi^{\gamma}_{2})$ and $(\psi^{\gamma}_{-3},\psi^{\gamma}_{3})$ describing the change of charge due to the π-orbital interactions. The corresponding deformation densities are given in Figure 5b as $\Delta\rho^{orb}_{\pi x}$ and $\Delta\rho^{orb}_{\pi x}$. The related stabilization energies are $\Delta E^{\pi x}_{orb} = \Delta E^{\pi y}_{orb} = (1)/(2)\Delta E^{\pi}_{orb} = -7.2$ kcal/mol; see Table 1. We note that ΔE^{π}_{orb} decreases in absolute terms for X_2H_6 from X = C to X = Sn as the X−X bond length increases and overlap between orbitals on the two XH_3 fragments diminish.

The results collected in Table 1 are in good qualitative agreement with experiment as well as with other theoretical investigations[98] based on the ETS scheme.

Double Bonds between the Main-Group Elements, $H_2X{=}XH_2$. Turning next to the double bonds between main group elements, we shall consider ethylene and its heavier homologue Ge_2H_4.[68,72−74] Planar ethylene with D_{2h} symmetry can be considered formed from two ground-state triplet carbenes $H_2C{\uparrow\uparrow}$ and $\downarrow\downarrow CH_2$ of opposite spin-polarization. The

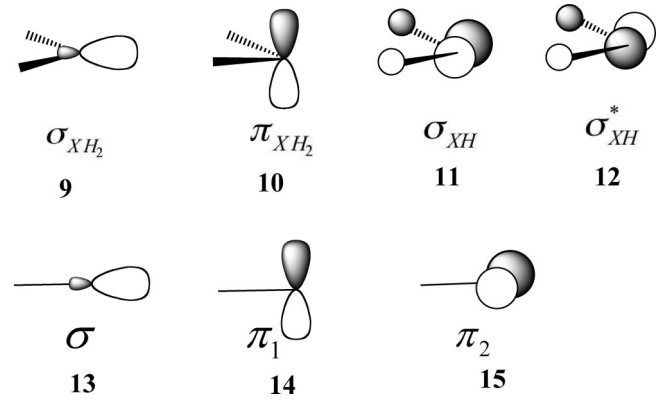

Figure 6. Schematic representation of XH_2 and XCH_3 fragment orbitals.

steric term ΔE_{steric} is somewhat larger for ethylene than for ethane because of the shorter C−C bond length, Table 2.

The carbene units[73−75] each have two singly occupied orbitals σ_{CH_2} (**9**) and π_{CH_2} (**10**); see Figure 6. They give rise to a σ- and a π-bond, respectively. In molecular orbital theory the σ-component is represented by σ_{CC} which is a bonding combination of σ_{CH_2} (**9**) on the two carbenes whereas the π-component is represented by π_{CC} which is the correspond-

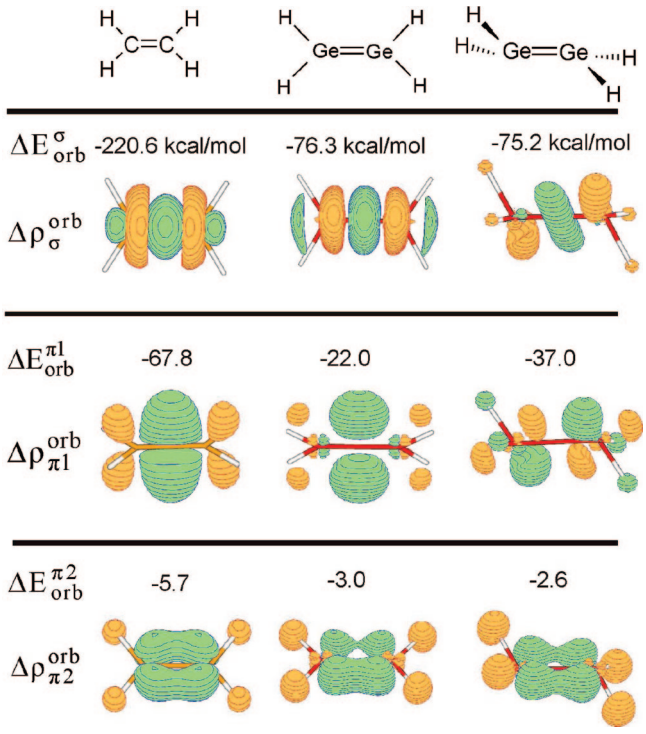

Figure 7. The contours of deformation density contributions $\Delta\rho_{\sigma}^{orb}$, $\Delta\rho_{\pi 1}^{orb}$, $\Delta\rho_{\pi 2}^{orb}$ for ethylene (left), hypothetical planar germanium system (middle), and the real trans-bent germanium homologue (right). The numerically smallest contour values are ±0.01 a.u. The last component, $\Delta\rho_{\pi 2}^{orb}$, was plotted with the contour values ±0.005 a.u. In addition the corresponding energies ΔE_{orb}^{σ}, $\Delta E_{orb}^{\pi 1}$, $\Delta E_{orb}^{\pi 2}$ are shown.

ing bonding combination of π_{CH_2} (**10**) on the two carbenes. The NOCVs for planar ethylene are given as Supporting Information. As for C_2H_6, bonds in C_2H_4 are formed by the shift of density from fragment A to B in one spin component and from B to A in the other component with a net buildup of charge in the bonding region. However, for C_2H_4 both a σ-components (σ_{CH_2}) and a π component (π_{CH_2}) is involved.

We present in the left-hand column of Figure 7 the contributions to the orbital interaction deformation density $\Delta\rho^{orb}$ from the σ- and π-bond as $\Delta\rho_{\sigma}^{orb}$ and $\Delta\rho_{\pi 1}^{orb}$, respectively, where we have summed over spin components. There is a noticeable accumulation of charge in the bonding region for both $\Delta\rho_{\sigma}^{orb}$ and $\Delta\rho_{\pi 1}^{orb}$. The corresponding contributions to ΔE_{orb} are given by $\Delta E_{orb}^{\sigma} = -220.6$ kcal/mol and $\Delta E_{orb}^{\pi 1} = -67.8$ kcal/mol, respectively. Thus our analysis finds in agreement with the common perception that the σ-bond is stronger than the π-bond. There is one more contribution to $\Delta\rho^{orb}$ and ΔE_{orb} given by $\Delta\rho_{\pi 2}^{orb}$ and$\Delta E_{orb}^{\pi 2}$, respectively. It is very similar to ΔE_{orb}^{π} of ethane and it involves the relief of Pauli repulsion by transferring density from the occupied and Pauli destabilized C−H bonding carbene fragment orbitals σ_{XH} (**11**) to the empty C−H antibonding carbene fragment orbitals σ_{XH}^{*} (**12**), see Figure 6. The stabilization amounts to $\Delta E_{orb}^{\pi 2} = -5.7$ kcal/mol.

Also presented in the second column of Figure 7 is planar Ge_2H_4 with triplet GeH_2 as the reference. The corresponding energy decomposition is given in Table 2. We find a reduction in both σ- and π-bond strength with $\Delta E_{orb}^{\sigma} = -76.3$ kcal/mol and $\Delta E_{orb}^{\pi 1} = -22.0$ kcal/mol as one would expect from the increase in the X−X bond distance in going from X = C to X = Ge. In reality Ge_2H_4[68,72] is trans-bent, Figure 7. Such a bending allows occupied Pauli destabilized and occupied spin−orbitals σ_{GeH_2} (**9**) on one fragment to overlap not only with empty σ_{GeH_2} orbitals on the other fragment but also with the corresponding empty π_{GeH_2} orbitals (**10**). As a result, $\Delta\rho_{\sigma}^{orb}$ for trans-bent Ge_2H_4 exhibits transfer of density from σ_{CH_2} to the bonding region; see third column of Figure 7. The bending allows as well occupied and Pauli-destabilized π_{GeH_2} spin−orbitals (**10**) on one fragment to interact not only with empty π_{GeH_2} orbitals on the other fragment but also with the corresponding empty σ_{GeH_2} orbitals (**9**). As a result $\Delta\rho_{\pi 1}^{orb}$ for trans-bent Ge_2H_4 exhibits some transfer of density from π_{GeH_2} to σ_{GeH_2}; see third column of Figure 7. It follows from Table 2 that $\Delta E_{orb}^{\sigma} = -75.2$ kcal/mol and $\Delta E_{orb}^{\pi 1} = -37.0$ kcal/mol, respectively, in the trans-bent conformation. Thus, the deformation from planarity slightly reduces the strength of the σ-bond while considerably strengthening the π-bond. Trans-bending is favorable when the overlap between the two π_{XH_2} orbitals is weak in the planar conformation of X_2H_4, as is increasingly the case through the heavier congeners of ethylene.

Strictly speaking, a σ/π separation is not possible when Ge_2H_4 is trans-bent. However, during the bending process, the ETS-NOCV scheme affords two major contributions to $\Delta\rho^{orb}$ (and ΔE_{orb}). Further, in the planar case these contributions correlate with $\Delta\rho_{\sigma}^{orb}$ and $\Delta\rho_{\pi}^{orb}$, respectively. We have for this reason maintained the same designation for the major components throughout the bending process. For the same reason we refer throughout to the two major contributions to ΔE^{orb} as $\Delta E_{orb}^{\pi 1}$ and $\Delta E_{orb}^{\pi 2}$, respectively. We note that $\Delta E_{orb}^{\pi 2}$, from the plane not influenced by the bending, is virtually unperturbed. We find it a useful characteristics of the ETS-NOCV scheme that the same basic components are maintained when the symmetry of the molecule is reduced.

In the case of GeH_2 the electronic ground-state is a singlet with two electrons in σ_{GeH_2} whereas π_{GeH_2} is empty. It is thus necessary to add a correction of 47.2 kcal /mol to ΔE_{prep} representing the difference in energy between the singlet and triplet states of two GeH_2 units. We might also perform the analysis of the bonding in X_2H_4 with the singlet state of XH_2 as the reference. However, the occupations of the σ_{XH_2} (**9**) and π_{XH_2} (**10**) orbitals in the final X_2H_4 complex is much closer to the triplet state of XH_2 than the singlet. This makes the triplet a natural choice. Nevertheless, it is important to underline that the bonding analysis depends on the reference. On the other hand, the relative energies of bent and planar species are invariant as are the bond energies as long as use is made of XH_2 in its electronic ground state.

Triple Bonds between the Main-Group Elements, RX≡XR. In order to demonstrate the application of the ETS-NOCV scheme to triple bonds between main group elements, we will discuss the X≡X bonding in RX≡XR, with R = CH_3 and X = C, Ge.

Let us start the discussion with the triple C≡C bond in the linear 2-butyne formed from the two units MeC↑↑↑ and ↓↓↓CMe having the opposite spin polarization. These units are each generated by promoting CMe from its doublet $^2E_y(\sigma^2\pi_{\lambda}^1;\gamma = 1,2)$ ground-state to its $^4A_2(\sigma^1\pi_1^1\pi_2^1)$ quartet

Table 3. ETS-NOCV Energy Decomposition of the Triple X≡X Bond in the RX≡XR Systems, R = CH_3, X = C, Ge[a]

X	ΔE_{steric}[b]	ΔE^{σ}_{orb}	$\Delta E^{\pi 1}_{orb}$	ΔE^{π}_{orb}[b]	ΔE^{π}_{orb}[b]	ΔE_{prep}[d]	ΔE_{int}[e]	d(XX)[f]
C	120.2	−209.7	−88.8	−88.8	−387.3	63.9	−203.18	1.21
Ge-linear	25.5	−102.1	−24.4	−24.1	−150.6	94.9	−30.2	2.20
Ge-bent	23.3	−104.5	−27.3	−34.2	−166.0	96.2	−46.5	2.29

[a] kcal/mol. [b] The total steric repulsion, $\Delta E_{steric} = \Delta E_{Pauli} + \Delta E_{elstat}$. [c] $\Delta E_{orb} = \Delta E^{\sigma}_{orb} + \Delta E^{\pi 1}_{orb} + \Delta E^{\pi 2}_{orb}$. [d] The distortion (or preparation) term includes the difference in energy between the doublet ground state and the excited quartet state of XH_2 fragments. [e] $\Delta E_{int} = \Delta E_{steric} + \Delta E_{prep} + \Delta E_{orb}$. [f] XX bond lengths in angstroms.

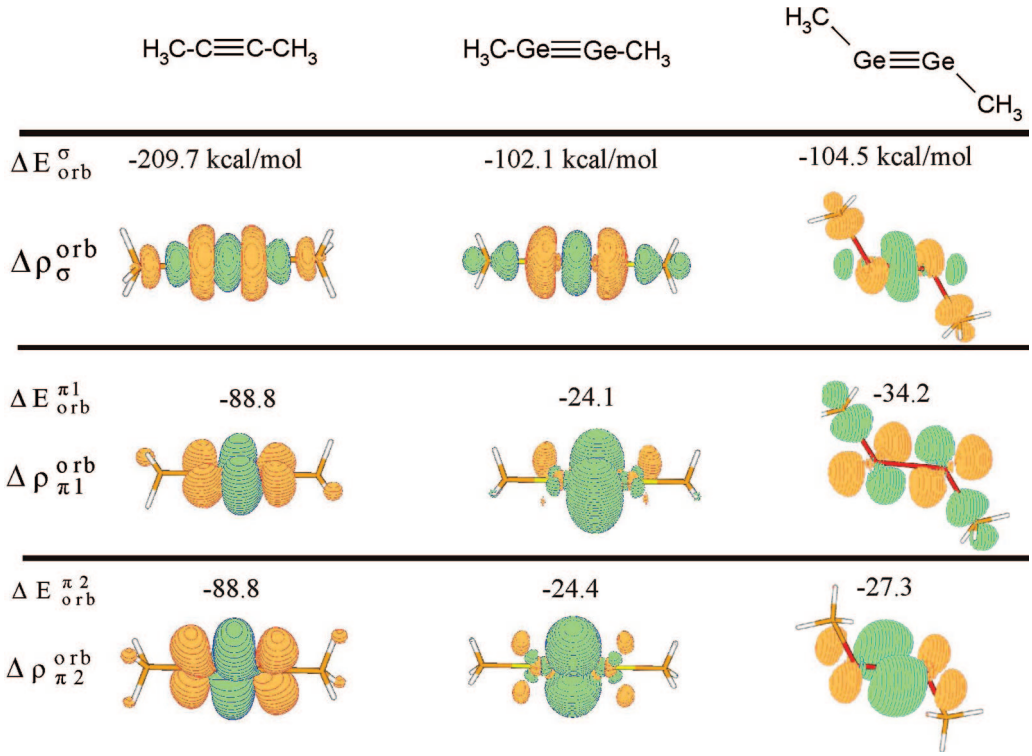

Figure 8. The contours of deformation density contributions $\Delta\rho^{orb}_{\sigma}$, $\Delta\rho^{orb}_{\pi 1}$, $\Delta\rho^{orb}_{\pi 2}$ for the triple bonds in the 2-butyne (left), hypothetical linear germanium system (middle), and the real trans-bent germanium homologue (right). The numerically smallest contour value are ±0.002 a.u. In addition the corresponding energies, ΔE^{σ}_{orb}, $\Delta E^{\pi 1}_{orb}$, $\Delta E^{\pi 2}_{orb}$ have been presented.

excited-state for the price of 63.2 kcal/mol for two CMe units. This energy is part of ΔE_{prep} given in Table 3.

The σ-component of the C≡C bond is made up from σ_A (**13**) and σ_B, on the two different fragments, H_3CC, CCH_3, respectively; see Figure 6. Similarly, the two equivalent π-type contributions to the C≡C bond are built from $\pi_{1,A}$ (**14**), $\pi_{2,A}$ (**15**), on one H_3CC fragment and $\pi_{1,B}$, $\pi_{2,B}$ of the second CCH_3 fragment; see Figure 6. The NOCVs representing the formation of the triple bond in $H_3CC{\equiv}CCH_3$ are given as Supporting Information. The deformation density contributions, $\Delta\rho^{orb}_{\sigma}$, $\Delta\rho^{orb}_{\pi 1}$, $\Delta\rho^{orb}_{\pi 2}$, representing the formation of one σ- and two π-components of the C≡C bond are shown in the left column of Figure 8. Also shown are the corresponding energies, ΔE^{σ}_{orb}, $\Delta E^{\pi 1}_{orb}$, $\Delta E^{\pi 2}_{orb}$. It is clear that the σ-bond contribution of $\Delta E^{\sigma}_{orb} = -209.7$ kcal/mol is stronger than the total π-bonding contribution given by $\Delta E^{\pi 2}_{orb} = -177.5$ kcal/mol.

Turning next to the corresponding $H_3CGe{\equiv}GeCH_3$ system, we promote in a way similar to acetylene the GeMe fragment from its doublet $^2E_\gamma$ ($\sigma^2\pi^1_\chi;\gamma = 1,2$) ground-state to its $^4A_2$ ($\sigma^2\pi^1_\chi\pi^1_\parallel$) quartet excited-state for the price of 94.9 kcal/mol for two GeMe units and add this contribution to ΔE_{prep} given in Table 3.

Considering first the $H_3CGe{\equiv}GeCH_3$ system with a linear structure, the σ- and π-contributions to ΔE_{orb} are significantly weaker (−102.1 and −24.4, −24.1, respectively) compared with 2-butyne, as it is shown in the middle column of Figure 8. This is directly related to the increase in the XX distance as we go from X = C to X = Ge; see the last column of Table 3.

Experimentally and theoretically the heavier alkyne homologues, RX≡XR, are known to adopt a trans-bent geometry.[75−84,90−94] The last column of Figure 8 indicates that the σ- and π-components, $\Delta\rho^{orb}_{\sigma}$, $\Delta\rho^{orb}_{\pi 2}$, of the Ge≡Ge bond in the bent-structure are slightly stronger (by 2.4, 2.9 kcal/mol, respectively) compared with the linear analogue. However, the second component of the Ge≡Ge bond, $\Delta E^{\pi 1}_{orb}$, exhibits the most significant increase in the strength, by 10.0 kcal/mol, compared with the linear system. In fact the bending makes it possible for the occupied and Pauli-destabilized π_1 orbital on one GeMe fragment to interact not only with the empty π_1 fragment orbital of the other fragment but also the corresponding empty σ component. The mixing appears as a donation of density from π_1 to σ in $\Delta\rho^{orb}_{\pi 1}$, Figure 8. We note again that we have used a σ/π notation for the contributions to $\Delta\rho^{orb}$ and ΔE_{orb} in trans-bent MeGe≡GeMe.

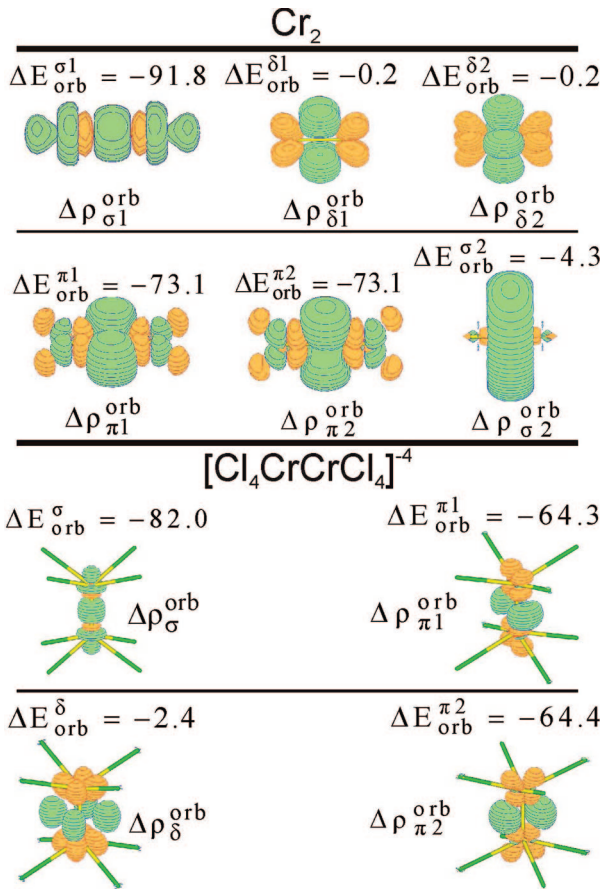

Figure 9. The contours of deformation density contributions describing the two σ-, two π-, and two δ-components of the hextuple bond in the Cr_2 dimer (upper part). The numerically smallest contour values are ±0.003 a.u. The only contour $\Delta\rho_{\sigma 2}^{orb}$ was plotted with the smaller contour values, ±0.001a.u., to improve the quality of visibility. In addition the deformation density components describing the quadruple bond in the $[Cl_4CrCrCl_4]^{4-}$ system have been displayed (lower part). The numerically smallest contour values are ±0.007 a.u. For all of the deformation density contributions, the corresponding energies have been presented.

It is again gratifying to see that the ETS-NOCV scheme affords a simple compact picture of the Ge≡Ge triple bond in terms of three components even when the σ/π separation is broken by distortions such as the trans-bent.

Multiple Bonds between the Metal Centers, Cr_2, Mo_2, W_2, $[Cl_4CrCrCl_4]^{4-}$. Up to now we have applied the ETS-NOCV scheme to a description of bonds between main-group elements. We shall next switch to a discussion of multiple bonds between metal centers. As the first (simple) example we consider the hextuple bonds in the dimers, X_2, with X = Cr, Mo, W. Each of the X_2 molecules was built from two atoms of opposite spin-polarization with the septet valence configuration ($nd_\sigma^1 nd_{\pi 1}^1 nd_{\pi 2}^1 nd_{\delta 1}^1 nd_{\delta 2}^1 (n+1)s^1$). The septet electronic configuration is the ground-state for chromium and molybdenium atoms whereas the quintet state is characteristic for tungsten.[87,92−94] Therefore we included in the total bonding term the energy describing the promotion from the ground quintet to the excited septet state for tungsten. Additionally, we will also characterize the quadruple Cr−Cr bond in the anion $[Cl_4CrCrCl_4]^{4-}$ with D_{4h} symmetry (eclipsed conformation) made up from the two $CrCl_4^{2-}$ fragments of C_{4v} symmetry each holding four unpaired electrons with the opposite spins and the $nd_\sigma^1 nd_{\pi 1}^1 nd_{\pi 2}^1 nd_\delta^1$ configuration. We found the quintet as a ground state for $CrCl_4^{2-}$ units.

The NOCV deformation density contributions from the components of the sextuple CrCr bond have been displayed in the upper part of Figure 9. Pairing of the five singly occupied *d*-orbitals on each metal center gives rise to one σ-, two π-, and the two δ-components represented by the $\sigma 1$, $\pi 1$, $\pi 2$, $\delta 1$, $\delta 2$ contributions to $\Delta\rho^{orb}$ andΔE_{orb}, Figure 9 and Table 4. We have in addition from $(n+1)s$ the $\sigma 2$ component.

The data presented in Table 4 for Cr_2 lead to the conclusion that the main energy contributions come from the total π-bonding, $\Delta E_{orb}^{\pi 1} + \Delta E_{orb}^{\pi 2} = -146.2$ kcal/mol, as well as $\sigma 1$ with $\Delta E_{orb}^{\sigma 1} = -91.8$ kcal/mol, whereas the δ-components ($\Delta E_{orb}^{\delta 1} + \Delta E_{orb}^{\delta 2} = -0.4$ kcal/mol) and the $\sigma 2$ component ($\Delta E_{orb}^{\sigma 2} = -4.3$ kcal/mol) from the 4*s* orbitals add very little to the bond strength. The same relative strengths of the bond-components can be found for the molybdenum and tungsten dimers. However, the total bond energy, ΔE_{tot}, increases (in absolute term) when going from the chromium (−31.3 kcal/mol) to the tungsten dimer (−88.7 kcal/mol). Similar conclusions were drawn from the experimental and as well as from the other theoretical investigations.[72,87−91] The factor responsible for the trend in ΔE_{int} is the steric repulsion, ΔE_{steric}. This term systematically decreases when chromium atoms are replaced by their group analogues. Further, the decrease in the steric repulsion is directly related to the decrease in the Pauli contribution, ΔE_{Pauli},[72] as the distance XX increase from X = Cr to X = W, the last column of Table 4. More precisely,[72] for chromium where 3*p*, 3*s*, and 3*d* are of the same radial extension, occupied 3*d* orbitals on one center experience Pauli repulsion from occupied 3*p*,3*s* orbitals on the other center. This effect is not present to the same extent for the heavier congeners where *ns*,*np* are much more contracted than *nd*.

Finally, let us briefly describe the character of the CrCr bond in $[Cl_4CrCrCl_4]^{4-}$. It follows from the lower part of Figure 9 that the four deformation density contributions, $\Delta\rho_\sigma^{orb}$, $\Delta\rho_{\pi 1}^{orb}$, $\Delta\rho_{\pi 2}^{orb}$, $\Delta\rho_\delta^{orb}$ with the corresponding energies ΔE_{orb}^{σ},$\Delta E_{orb}^{\pi 1}$, $\Delta E_{orb}^{\pi 2}$, ΔE_{orb}^{δ} accounts for the formation of the Cr−Cr bond in $[Cl_4CrCrCl_4]^{4-}$. Again, the largest contributions to the strength of the quadruple Cr−Cr bond come from the σ- and π-bonding whereas the δ-component is the weakest. We note that the term ΔE_{steric} in $[Cl_4CrCrCl_4]^{4-}$ also contains the coulomb interaction V_{AB} between the two net charges ($q = -2$) on the two $[Cl_4Cr]^{2-}$ fragments as discussed in the theoretical section in connection with the introduction of ΔE_{steric} near eq 10.

Multiple Bonds between Main-Group Elements and Metal Center, $(CO)_5Cr{=}XH_2$. The analysis up to now has been of bonds between either two main-group elements or two metal centers. We shall in this section apply the ETS-NOCV scheme to bonds between transition metals and main-group elements. Consider to this end the carbene-type complex $Cr(CO)_5XH_2$ (with X = C, Si, Ge, Sn). Let the complex further be formed from the square pyramidal metal

Table 4. ETS-NOCV Energy Decomposition of the Hextuple Bond in the X_2 Dimers (X = Cr, Mo, W) and the Quadruple Bond in the $[Cl_4CrCrCl_4]^{4-}$ Molecule[a]

X	ΔE_{orb}^{σ}[a]	ΔE_{orb}^{σ}[b]	ΔE_{orb}^{π}[a]	ΔE_{orb}^{π}[b]	ΔE_{orb}^{δ}[a]	ΔE_{orb}^{δ}[b]	ΔEsteric[b]	ΔE_{int}[c]	d(XX)[d]
Cr_2	−91.8	−4.3	−73.1	−73.1	−0.2	−0.2	211.4	−31.3	1.64
Mo_2	−90.0	−6.7	−74.7	−74.7	−2.5	−2.5	173.2	−77.9	1.98
W_2	−74.2	−13.8	−75.0	−75.0	−5.7	−5.7	150.7	−88.7[e]	2.04
$[Cl_4CrCrCl_4]^{4-}$	−82.0	–	−64.3	−64.4	−2.4	–	189.0	−24.1	1.88

[a] kcal/mol. [b] The total steric repulsion, $\Delta E_{steric} = \Delta E_{Pauli} + \Delta E_{elstat}$. [c] $\Delta E_{int} = \Delta E_{steric} + \Delta E_{prep} + \Delta E_{orb}$, $\Delta E_{orb} = \Delta E_{orb}^{\sigma 1} + \Delta E_{orb}^{\sigma 2} + \Delta E_{orb}^{\delta 1} + \Delta E_{orb}^{\sigma 2} + \Delta E_{orb}^{\pi 1} + \Delta E_{orb}^{\pi 2}$. [d] XX bond lengths in angstroms. [e] For W_2 the term ΔE_{int} includes 10.0 kcal/mol from the promotion of the quintet ground state of the tungsten atoms to their septet excited states.

Table 5. ETS-NOCV Energy Decomposition of the Double Bond in the $(CO)_5Cr{=}XH_2$ complexes[a]

X	ΔE_{steric}[b]	ΔE_{orb}^{σ}	ΔE_{orb}^{π}	ΔE_{orb}	ΔE_{prep}	ΔE_{int}[c]	$\Delta E_{HOMO/LUMO}$[d]
C	20.6	−51.9	−46.3	−98.2	19.0[e]	−58.6	1.42
Si	23.7	−55.9	−19.0	−74.9	3.8	−47.4	1.67
Ge	21.7	−51.8	−15.4	−67.2	4.3	−41.2	2.49
Sn	13.5	−45.6	−9.7	−55.3	4.5	−37.3	2.63

[a] kcal/mol. [b] The total steric repulsion, $\Delta E_{steric} = \Delta E_{Pauli} + \Delta E_{elstat}$. [c] $\Delta E_{int} = \Delta E_{steric} + \Delta E_{prep} + \Delta E_{orb}$, $\Delta E_{orb} = \Delta E_{orb}^{\sigma} + \Delta E_{orb}^{\pi}$. [d] The difference in energies (eV) between occupied d_π of $Cr(CO)_5$ and the LUMO π_{XH_2}. [e] Distortion term includes the difference in energy between the triplet ground state and the singlet excited state of CH_2 fragment.

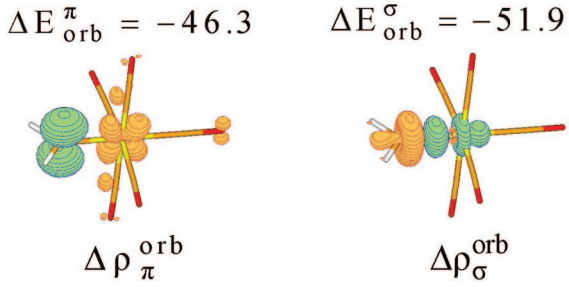

Figure 10. The contours of deformation density contributions $\Delta\rho_\sigma^{orb}$, $\Delta\rho_\pi^{orb}$ describing the σ- and π-components of the carbene bond in the $(CO)_5Cr{=}CH_2$ complex together with the corresponding energies ΔE_σ^{orb}, ΔE_π^{orb}. The numerically smallest contour values are ±0.01 a.u.

fragment $Cr(CO)_5$ with a low-spin d^6 ground-state configuration and the XH_2 ligand in its singlet state. For CH_2, the ground state is a triplet and we must add 15.5 kcal/mol to ΔE_{prep}; see Table 5.

Figure 10 exhibits the leading deformation density contributions $\Delta\rho_\pi^{orb}$ and $\Delta\rho_\sigma^{orb}$ together with the corresponding energies, ΔE_{orb}^{π}, ΔE_{orb}^{σ}. The σ-bond contribution $\Delta\rho_\sigma^{orb}$ is due to donation from the occupied σ_{CH_2} orbital into the empty d_{z2} orbital of the metal-based fragment, with d_{z2} pointing toward the carbene. The associated σ-bond formation energy is $\Delta E_{orb}^{\sigma} = -51.9$ kcal/mol. The second component, $\Delta\rho_\pi^{orb}$, represents the π-back-donation from an occupied d_π orbital of the metal into the empty π_{CH_2} type orbital of CH_2. The corresponding energy is given by $\Delta E_{orb}^{\pi} = -46.3$ kcal/mol.

The σ-bond strength ΔE_{orb}^{σ} is seen to change little along the homologue series X = C, Si, Ge. On the other hand, the π-bond strength ΔE_{orb}^{π} is much larger for X = C than for the other elements, Table 5, as the overlap between d_π and π_{XH_2} drops sharply from X = C to X = Si because of the increased Cr−X bond distance. Further, ΔE_{orb}^{π} decreases steadily from X = Si to X = Sn as the energy gap between d_π and π_{XH_2} increases, Table 5.

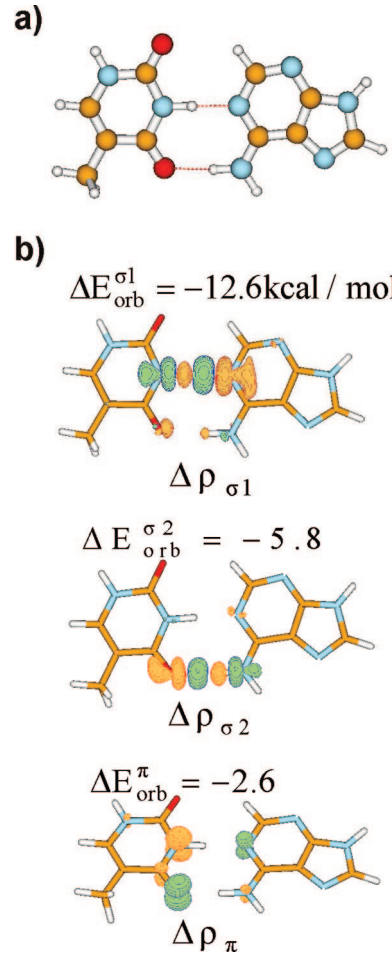

Figure 11. The adenine and thymine fragments in the base pair between the two nucleobases (panel a). The contours of the deformation densities describing the NH−N ($\Delta\rho_{\sigma 1}$) and NH−O ($\Delta\rho_{\sigma 2}$) hydrogen bonds as well as the π-resonance ($\Delta\rho_\pi$). Also shown are the corresponding energy contributions, $\Delta E_{orb}^{\sigma 1}$, $\Delta E_{orb}^{\sigma 2}$, ΔE_{orb}^{π} (panel b). The numerically smallest contour values are ±0.01 a.u.

Our bond analysis of $Cr(CO)_5XH_2$ conforms to the known Dewar−Chatt−Duncanson model[85,86] with σ-donation from σ_{XH_2} to d_{z2} and π-back-donation from d_π to π_{XH_2}. We find that the charge involved in the σ_{XH_2} to d_{z2} donation is 0.92 (C), 0.83 (Si), 0.81 (Ge), and 0.80 (Sn) whereas the corresponding numbers for the d_π to π_{XH_2} π-back-donation are 0.77 (C), 0.65 (Si), 0.53 (Ge), and 0.40 (Sn).

The Hydrogen Bond in Deoxyribonucleic Acid (DNA) between Nucleobases. We shall as another example of a donor−acceptor interaction briefly consider the hydrogen bond in DNA between two nucleobases typified by the

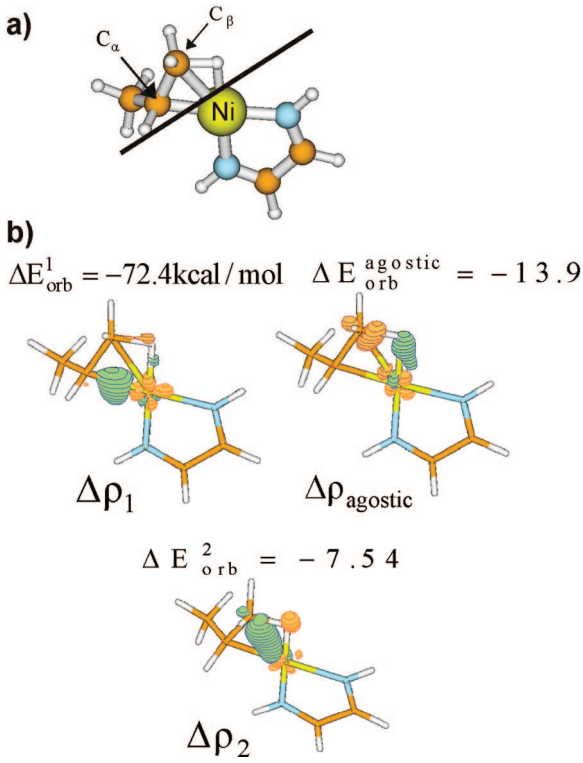

Figure 12. (a) Definition of the fragment separation in the β-agostic propyl-based complex. (b) The contours of the deformation densities describing the two σ bonds (C_α-Ni, $\Delta\rho 1$), ($C\beta$-Ni, $\Delta\rho 2$), and the agostic interaction ($C\beta H\cdots Ni$, $\Delta\rho_{agostic}$). Also shown are the corresponding energy contributions, ΔE^1_{orb}, ΔE^2_{orb}, $\Delta E^{agostic}_{orb}$. The numerically smallest contour values are ± 0.01 a.u. for $\Delta\rho_1$ and $\Delta\rho_{agostic}$. The corresponding values for $\Delta\rho_2$ are ± 0.005 a.u.

Table 6. ETS-NOCV Energy Decomposition Results for the Adenine-Thymine Base Pair (A-T)

BP86/TZ2P	kcal/mol
ΔE_{int}	−13.0
ΔE_{orb}	−22.0
ΔE_{Pauli}	38.7
ΔE_{prep}	2.1
ΔE_{elstat}	−31.9
ΔE_{int} (experiment)[99]	−12.1
ΔE_{int} (other theoretical results)[100]	−13.2

adenine-thymine base pair, Figure 11a. This system has previously been studied both experimentally[99] and theoretically.[100] It follows from Figure 11b that three deformation density components ($\Delta\rho_{\sigma 1}$, $\Delta\rho_{\sigma 2}$, $\Delta\rho_\pi$) contribute to the A-T bonding. The energetically most important contributions ($\Delta E^{\sigma 1}_{orb}$, $\Delta E^{\sigma 2}_{orb}$) come from the donor−acceptor interactions ($\Delta\rho_{\sigma 1}$, $\Delta\rho_{\sigma 2}$) between the occupied lone pairs of oxygen (from thymine) and nitrogen (from adenine) and the two unoccupied σ^* orbitals of the N−H bonds. We note that the hydrogen bond involving the nitrogen lone pair ($\Delta\rho_{\sigma 1}$) has a more stabilizing contribution with $\Delta E^{\sigma 1}_{orb} = -12.6$ kcal/mol compared to $\Delta\rho_{\sigma 2}$ involving the oxygen lone pair for which $\Delta E^{\sigma 2}_{orb} = -5.8$ kcal/mol, Figure 11b and Table 6. This is in line with the fact that nitrogen is the better donor. The deformation density $\Delta\rho_\pi$ illustrates the minor participation of π-type orbitals in the A-T bonding. Thus density depletion in the σ-network gives rise to density buildup in the π-framework and visa versa. This so-called Resonance Assisted Hydrogen Bonding (RAHB)[100] between the adenine and thymine subsystems amounts to $\Delta E^{\pi}_{orb} = -2.6$ kcal/mol. Hydrogen bonding in the A-T pair has already been fully analyzed and understood in a previous ETS study.[100] However, the analysis given here illustrate that the ETS-NOCV scheme is able to capture the essential bonding aspects in a few plots as illustrated in Figure 11b. The theoretical bond energies presented in Table 6 are seen to be in good agreement with experiment.

Agostic Bond Interactions in Transition Metal Alkyl Complexes. We shall as our last example study the agostic bonding interactions in a nickel-based β-agosctic propyl complex[101] formed between a C_β−H bond of the propyl group and a nickel center (Figure 12a). It is clear from Figure 12b that three components ($\Delta\rho_1$, $\Delta\rho_2$, $\Delta\rho_{agostic}$) are present in the bond between the propyl group and the nickel center. The dominant contribution, $\Delta\rho_1$, with $\Delta E^1_{orb} = -72.4$ kcal/mol comes from the σ-bond formed between C_α of the propyl group and the nickel center. The second energetically relevant component, $\Delta\rho_{agostic}$, with $\Delta E^{agostic}_{orb} = -13.9$ kcal/mol describes the β-agostic interaction between the C_β−H bond and nickel. Finally, the last component, $\Delta\rho_2$, exhibits direct formation of a weak C_β−Ni σ-bond, with $\Delta E^2_{orb} = -7.54$ kcal/mol. We should point out that a very useful feature of the ETS-NOCV scheme is that we can separate (and simultaneously quantify) the β-agostic interaction between the C_β−H bond of propyl ($\Delta\rho_{agostic}$) from the two Ni−C sigma bonds ($\Delta\rho_1$, $\Delta\rho_2$).

Concluding Remarks

In the present study we have combined the Extended Transition State (ETS) scheme with the Natural Orbitals for Chemical Valence (NOCV) method. It has been shown that the ETS-NOCV charge and energy decomposition scheme offers a compact picture of chemical bond formation within one common theoretical framework. Thus, it not only makes it possible to obtain a qualitative picture of the different components of the chemical bond (σ, π, δ, etc.) by visualization of the deformation density contributions, $\Delta\rho_k$, but it also provides the corresponding quantitative energies, ΔE^{orb}_k. Although, our description of bonding is based on a subjective division of a molecule into subsystems (fragments) with a particular electronic structure, we have demonstrated the applicability of the ETS-NOCV scheme in a description of various types of chemical bonds. They include single, double, and triple bonds between main group elements, sextuple and quadruple bonds between metal centers, and double bonds between a metal and a main group element.

The ETS scheme has previously been used to extract the various components (σ, π, δ, etc.) of the chemical bond for highly symmetrical molecules where ΔE_{orb} is blocked by symmetry.[20−22,25−27,59−62] However, without high symmetry such a separation into the σ, π, δ components was not possible. The distinctive advantage of the new ETS-NOCV charge and energy decomposition scheme is that we do not need a specific point group symmetry for a given molecule to assess the σ, π, δ contributions to the chemical bond. In

fact they can be easily identified by visualization of the deformation density contributions, $\Delta\rho_k$, and quantified by providing the corresponding energies, ΔE_k^{orb}, (see eq 17), even for molecules with no symmetry. Accordingly ETS and NOCV combined significantly broadens the spectrum of applications for the ETS scheme. We have here illustrated the applicability of the ETS-NOCV scheme with applications ranging from strong single and multiple bonds to weak hydrogen bonding interactions.

Acknowledgment. This work was supported by NSERC as well as a research grant from the Polish Ministry of Science and Higher Education in Poland (N N204 227534). T.Z. thanks the Canadian Government for a Canada Research Chair.

References

(1) Lewis, G. N. *J. Am. Chem. Soc.* **1916**, *38*, 762.

(2) Heitler, W.; London, F. *Z. Phys.* **1927**, *44*, 455.

(3) Shaik, S.; Hilberty, P. C. *Rev. Comput. Chem.* **2004**, *20*, 1.

(4) Mulliken, R. S. *Phys. Rev.* **1932**, *40*, 55.

(5) Hückel, E. *Trans. Faraday Soc.* **1934**, *30*, 59.

(6) Jug, K. *J. Am. Chem. Soc.* **1977**, *99*, 7800.

(7) Jug, K. *J. Am. Chem. Soc.* **1978**, *100*, 6581.

(8) Foster, J. P.; Weinhold, F. *J. Am. Chem. Soc.* **1980**, *102*, 7211.

(9) Reed, A. E.; Weinhold, F. *J. Chem. Phys.* **1985**, *83*, 1736.

(10) Reed, A. E.; Weinhold, F. *J. Chem. Phys.* **1983**, *78*, 4066.

(11) Reed, A. E.; Weinhold, F. *J. Chem. Phys.* **1986**, *84*, 5687.

(12) Reed, A. E.; Curtiss, L. A.; Weinhold, F. *Chem. Rev.* **1998**, *88*, 899.

(13) Bader, R. F. W. *Atoms in Molecules. A Quantum Theory*; University Press: Oxford, 1990.

(14) Becke, A.; Edgecombe, K. E. *J. Chem. Phys.* **1990**, *92*, 5397.

(15) Esterhuysen, C.; Frenking, G. *Theoret. Chem. Acc.* **2004**, *111*, 381.

(16) Coppens, P. *Electron Distribution and the Chemical Bond*; Plenum Press: New-York, 1982.

(17) Löwdin, P. O. *J. Chem. Phys.* **1950**, *18*, 365.

(18) Mulliken, R. S. *J. Chem. Phys.* **1955**, *23*, 1833.

(19) Dapprich, S.; Frenking, G. *J. Phys. Chem.* **1995**, *99*, 9352.

(20) Frenking, G.; Fröhlich, N. *Chem. Rev.* **2000**, *100*, 717.

(21) Frenking, G.; Wichmann, K.; Fröchlich, N.; Grobe, J.; Golla, W.; Le Van, D.; Krebs, B.; Läge, M. *Organometallics* **2002**, *21*, 2921.

(22) Frenking, G. *Science* **2005**, *310*, 796.

(23) Frenking, G.; Loschen, C.; Krapp, A.; Fau, S.; Strauss, S. H. *J. Comput. Chem.* **2006**, *28*, 117.

(24) Kitaura, K.; Morokuma, K. *Int. J. Quantum Chem.* **1976**, *10*, 325.

(25) Ziegler, T.; Rauk, A. *Theor. Chim. Acta* **1977**, *46*, 1.

(26) Ziegler, T.; Rauk, A. *Inorg. Chem.* **1979**, *18*, 1755.

(27) Ziegler, T.; Rauk, A. *Inorg. Chem.* **1979**, *18*, 1558.

(28) Mo, Y.; Gao, J.; Peyerimhoff, S. D. *J. Chem. Phys.* **2000**, *112*, 5530.

(29) Khaliullin, R. Z.; Cobar, E. A.; Lochan, R. C.; Bell, A. T.; Head-Gordon, M. *J. Phys. Chem. A* **2007**, *111*, 8753.

(30) Schenter, G. K.; Glendening, E. D. *J. Phys. Chem.* **1996**, *100*, 17152.

(31) Fransisco, E.; Pendás, M.; Blanco, M. A. *J. Chem. Theory Comput.* **2006**, *2*, 90.

(32) Mayer, I.; Hamza, A. *Int. J. Quantum Chem.* **2005**, *103*, 798.

(33) Korchowiec, J.; Uchimaru, T. *J. Chem. Phys.* **2000**, *112*, 1623.

(34) Liu, S., Govind, N. *J. Phys. Chem. A* 2008.

(35) Bagus, P. S.; Hermann, K.; Bauschlicher, C. W. *J. Chem. Phys.* **1984**, *80*, 4378.

(36) Jeziorski, B.; Moszynski, R.; Szalewicz, K. *Chem. Rev* **1994**, *94*, 1887.

(37) SAPT96 is an ab initio program for many-body symmetry adapted perturbation theory calculations of intermolecular interaction written by Bukowski, R.; Jankowski, P.; Jeziorski, B; Jeziorski, M.; Kucharski, S. A.; Moszynski, R.; Rybak, S; Szalewicz, K.; Williams, H. L.; Wormer, P. E. S. University of Delaware and University of Warsaw, 1996.

(38) Pauling, L. *The nature of the chemical bond*; Cornell Univ. Press: Ithaca, 1941.

(39) Wiberg, K. *Tetrahedron* **1968**, *24*, 1093.

(40) Gopinathan, M. S.; Jug, K. *Theoret. Chim. Acta* **1983**, *63*, 497.

(41) Mayer, I. *Chem. Phys. Lett.* **1984**, *97*, 270.

(42) Ciosłowski, J.; Mixon, S. T. *J. Am. Chem. Soc.* **1991**, *113*, 4142.

(43) Nalewajski, R. F.; Köster, A. M.; Jug, K. *Theor. Chim. Acta* **1993**, *85*, 463.

(44) Nalewajski, R. F.; Mrozek, J. *Int. J. Quantum Chem.* **1994**, *51*, 187.

(45) Nalewajski, R. F.; Mrozek, J.; Formosinho, S. J.; Varandas, A. J. C. *Int. J. Quantum Chem.* **1994**, *52*, 1153.

(46) Nalewajski, R. F.; Mrozek, J.; Mazur, G. *Can. J. Chem.* **1996**, *74*, 1121.

(47) Nalewajski, R. F.; Mrozek, J.; Michalak, A. *Int. J. Quantum Chem.* **1997**, *61*, 589.

(48) Nalewajski, R. F.; Mrozek, J.; Michalak, A. *Pol. J. Chem.* **1998**, *72*, 1779.

(49) Michalak, A.; De Kock, R.; Ziegler, T. *J. Phys. Chem. A,* **2008**, *112*, 7256.

(50) Michalak, A.; Mitoraj, M.; Ziegler, T. *J. Phys. Chem. A.* **2008**, *112* (9), 1933.

(51) Mitoraj, M.; Michalak, A. *Organometallics* **2007**, *26* (26), 6576.

(52) Mitoraj, M.; Michalak, A. *J. Mol. Model.* **2007**, *13*, 347.

(53) Mitoraj, M.; Michalak, A. *J. Mol. Model.* **2008**, *14*, 681.

(54) Mitoraj, M.; Zhu, H.; Michalak, A.; Ziegler, T. *Int. J. Quantum Chem*. 2008, DOI:, 10.1002/qua.21910.

(55) Löwdin, P. O. *J. Chem. Phys.* **1950**, *18*, 364.

(56) Pakiari, A. H.; Fakhraee, S.; Azami, S. M. *Int. J. Quantum Chem.* **2008**, *108*, 415.

(57) Hurley, A. C. *J. Chem. Phys.* **1962**, *37*, 449.

(58) TeVelde, G.; Bickelhaupt, F. M.; Baerends, E. J.; Fonseca Guerra, C.; Van Gisbergen, S. J. A.; Snijders, J. G.; Ziegler, T. *J. Comput. Chem.* **2001**, *22*, 931, and refs therein.

(59) Baerends, E. J.; Ellis, D. E.; Ros, P. *Chem. Phys.* **1973**, *2*, 41.

(60) Baerends, E. J.; Ros, P. *Chem. Phys.* **1973**, *2*, 52.

(61) te Velde, G.; Baerends, E. J. *J. Comput. Phys.* **1992**, *99*, 84.

(62) Fonseca, C. G.; Visser, O.; Snijders, J. G.; te Velde, G.; Baerends, E. J. In *Methods and Techniques in Computational Chemistry*; METECC-95; Clementi, E., Corongiu, G., Eds.; STEF: Cagliari, Italy, 1995; p 305.

(63) Becke, A. *Phys. Rev. A* **1988**, *38*, 3098.

(64) Perdew, J. P. *Phys. Rev. B* **1986**, *34*, 7406.

(65) van Lenthe, E.; Baerends, E. J.; Snijders, J. G. *J. Chem. Phys.* **1993**, *99*, 4597.

(66) van Lenthe, E.; Baerends, E. J.; Snijders, J. G. *J. Chem. Phys.* **1993**, *101*, 9783.

(67) van Lenthe, E.; van Leeuwen, R.; Baerends, E. J.; Snijders, J. G. *Int. J. Quantum Chem.* **1996**, *57*, 281.

(68) Jacobsen, H.; Ziegler, T. *J. Am. Chem. Soc.* **1994**, *116*, 3667.

(69) Bickelhaupt, F. M.; Baerends, E. J. Kohn-Sham Density Functional Theory: Predicting and Understanding Chemistry. *Reviews in Computational Chemistry*; Lipkowitz, K. B., Boyd, D. B., Eds.; Wiley-VCH: New York, 2000; Vol. 15, pp 1−86.

(70) Mitoraj, M.; Zhu, H.; Michalak, A.; Ziegler, T. *J. Org. Chem.* **2006**, *71*, 9208.

(71) Mitoraj, M.; Zhu, H.; Michalak, A.; Ziegler, T. *Organometallics* **2007**, *26*, 1627.

(72) Ziegler, T. Periodic Trends in Bond Energies: A Density Functional Study In *Computational Thermochemistry ACS Symposium Series 677*; Irikura, K. K., Frurip, D. J., Eds.; American Chemical SocietyWshington, DC, 1998; pp 369−383.

(73) Wagman, D. D.; Evans, W. H.; Parker, V. B.; Schumm, R. H.; Halow, I.; Bailey, S. M.; Churney, K. L.; Nuttall, R. L. *J. Phys. Chem. Ref. Data* **1982**, *11* (suppl. 2), xxx–xxx.

(74) Langhoff, S. A.; Bauschlicher, C. W., Jr.; Taylor, P. W. *Chem. Phys. Lett.* **1991**, *180*, 88.

(75) Pu, L.; Twamley, B.; Power, P. P. *J. Am. Chem. Soc.* **2000**, *122*, 3524.

(76) Phillips, A. D.; Wright, R. J.; Olmstead, M. M.; Power, P. P. *J. Am. Chem. Soc.* **2002**, *124*, 5930.

(77) Stender, M.; Phillips, A. D.; Wright, R. J.; Power, P. P. *Angew. Chem., Int. Ed.* **2002**, *41*, 1785.

(78) Wiberg, N.; Niedermayer, W.; Fischer, G.; Noth, H.; Suter, M. *Eur. J. Inorg. Chem.* **2002**, 1066.

(79) Sekiguchi, A.; Kinjo, R.; Ichinohe, M. *Science (Washington, DC)* **2004**, *305*, 1755.

(80) Pignedoli, C. A.; Curioni, A.; Andreoni, W. *ChemPhysChem* **2005**, *6*, 1795.

(81) Malcolm, N. O. J.; Gillespie, R. J.; Popelier, P. L. A. *J. Chem. Soc., Dalton Trans.* **2002**, 3333.

(82) Allen, T. L.; Fink, W. H.; Power, P. P. *J. Chem. Soc., Dalton Trans.* **2000**, 407.

(83) Bridgeman, A. J.; Ireland, L. R. *Polyhedron* **2001**, *20*, 2841.

(84) Jung, Y.; Brynda, M.; Power, P.; Head-Gordon, M. *J. Am. Chem. Soc.* **2006**, *128*, 7185.

(85) Dewar, M. J. S. *Bull. Soc. Chim.* **1951**, *18*, C71.

(86) Chatt, J.; Duncanson, J. A. *J. Chem. Soc.* **1953**, *3*, 2939.

(87) Thomas, E. J.; Murray, J. S.; O'Connor, C. J.; Politzer, P. *J. Mol. Struct.* **1999**, *487*, 177.

(88) Roos, B. O. *Collect. Czech. Chem. Commun.* **2003**, *68*, 265.

(89) Roos, B. O.; Borin Antonio, C.; Gagliardi, L. *Angew. Chem., Int. Ed.* **2007**, *46*, 1469.

(90) Bondybey, V. E.; English, J. H. *Chem. Phys. Lett.* **1983**, *94*, 443. Takagi, N.; Nagase, S. *Organometallics* **2007**, *26*, 469.

(91) Simard, B.; Lebeault-Dorget, M.-A.; Marijnissen, A.; Meulen, J. J. *J. Chem. Phys.* **1998**, *108*, 9668. Takagi, N.; Nagase, S. *Organometallics* **2007**, *26*, 3627.

(92) Sugiyama, Y.; Sasamori, T.; Hosoi, Y.; Furukawa, Y.; Takagi, N.; Nagase, S.; Tokitoh, N. *J. Am. Chem. Soc.* **2006**, *128*, 1023. Pis Diez, R. *Int. J. Quantum Chem.* **2000**, *76*, 105.

(93) Balasubramanian, K.; Dingguo, D. *Chem. Phys. Lett.* **1997**, *265*, 538.

(94) Radius, U.; Breher, F. *Angew. Chem., Int. Ed.* **2006**, *45*, 3006.

(95) Lai, C.-H.; Su, M.-d. *J. Comput. Chem.* **2008**, *29*, 2487.

(96) Nalewajski, R. F.; Korchowiec, J.; Michalak, A. In *Reactivity Criteria in Charge Sensitivity Analysis*; Nalewajski, R. F., Ed.;Topics in Current Chemistry, Vol. *183*: Density Functional Theory - Theory of Chemical Reactivity; Springer-Verlag: Heidelberg, 1996; pp 25−141.

(97) Nalewajski, R. F. *J. Math. Chem.* **2008**, *44*, 802.

(98) Kovàcs, A.; Esterhuysen, C.; Frenking, G. *Chem. Eur. J.* **2005**, *11*, 1813.

(99) Yanson, K.; Teplitsky, A. B.; Sukhodub, L. F. *Biopolymers* **1979**, *18*, 1149.

(100) Guerra, C. F.; Bickelhaupt, F. M.; Snijders, J. G.; Baerends, E. J. *Chem. Eur. J.* **1999**, *5*, 3581.

(101) Johnson, L. K.; Mecking, S.; Brookhart, M. *J. Am Chem Soc.* **1996**, *118*, 267.

CT800503D